phys. stat. sol. (a) **205**, No. 7, 1566–1571 (2008) / **DOI** 10.1002/pssa.200824117

physica status solidi a
www.pss-a.com
applications and materials science

A morphological and microstructural study of flame-sprayed zinc coatings on low-alloyed steels as a contribution to explaining their corrosion resistance

D. Chaliampalias, G. Vourlias, N. Pistofidis, G. Stergioudis, and E. K. Polychroniadis*

Physics Department, Aristotle University of Thessaloniki, 54124 Thessaloniki, Greece

Received by S. T. Lee 23 October 2007, revised 18 December 2007, accepted 20 March 2008
Published online 28 May 2008

PACS 61.05.cp, 68.37.Hk, 68.37.Lp, 81.15.Rs, 81.65.Kn, 81.65.Mq

* Corresponding author: e-mail polychr@auth.gr, Phone: +30 2310 99 8163, Fax: +30 2310 99 8241

Zinc is an ideal coating material for steels because it offers simultaneously cathodic and barrier protection. Several processes have been developed to provide zinc coatings. Thermal spraying is widely used due to the fact that it is simple, quick and effective. The present work deals with the morphology, the structure and the corrosion performance of zinc coatings deposited with thermal spraying. The study was performed with scanning electron microscopy and X-ray diffraction, while microstructural characterization was accomplished with transmission electron microscopy. Finally, corrosion tests were performed with exposure of the coated samples in a salt-spray chamber. From the microstructural investigation it was deduced that before corrosion the as-produced coatings are mainly composed of zinc, while zinc oxide nanoparticles are dispersed in their mass. After corrosion tests it was found that zinc flame-sprayed coatings provide adequate corrosion protection because the corrosive elements did not penetrate the coating or reach the substrate.

1 Introduction One of the most important products of the worldwide metal production is zinc [1]. The increased demand for this metal is mainly due to its application as a corrosion resistant coating for ferrous materials. This property is attributed to its position in the electromotive series of metals, which indicates that zinc provides sacrificial protection due to the fact that it is cathodic to steel [1]. At the same time it prevents contact between the underlying steel and the environment (barrier protection) as it reacts with atmospheric compounds (O_2, CO_2 and H_2O) and forms on its surface an adherent and water-insoluble film.

Several methods have been developed for zinc deposition as Table 1 indicates. The most usual is hot-dip galvanizing, which is the predominant on the industrial scale [1]. Another promising method is thermal spraying (metallizing). In this case, metallic zinc in the form of powder or wire is fed to a torch, where it is heated to its melting point by the combustion of an oxygen-acetylene fuel gas or by an electric arc. The resulting molten or nearly molten droplets are accelerated by a gas stream and projected against the surface to be coated (i.e. the substrate). On impact the droplets flow into thin particles adhering to the surface, which overlap and interlock as they solidify [2–6]. The total coating thickness is usually generated in multiple passes of the coating device.

Metallizing can be applied to ferrous materials of nearly any size. However, abrasive cleaning of the steel is required prior to the coating procedure, while sealing of the final coating with a low viscosity organic liquid such as silicone or polyurethane oil is necessary due to high porosity [7]. But these disadvantages are insignificant, because zinc metallizing is characterized by very high versatility as it does not require special installations and it is also applicable in the field. This is in contrast to the competitive techniques that are applicable only in the workshop and therefore are, in many cases, not practical. Furthermore, it provides much thicker coatings suitable for very aggressive environments such as marine. For this purpose the present work, as far as corrosion is concerned, focuses on the phenomena that take place in marine atmospheres.

Table 1 Major deposition techniques of metallic zinc coatings.

principle	commercial method
immersion in a molten zinc bath	hot-dip galvanizing
immersion in a chemical bath	electroplating
spraying of molten zinc	thermal spraying (metallizing)
chemical vapor deposition	pack cementation/fluidized-bed reactor

However, the structure and the morphology of the as-deposited coatings have not been sufficiently studied. The available information concerns only their composition and their thickness [8], while there is no data regarding the phases present in their mass, due to possible interactions between the coating and the substrate. By contrast, the corrosion of these coatings is compared with the behavior of zinc coatings deposited with other methods [9–12] and it is deduced that the corrosion mechanism depends on the coating method. Hence, the aim of the present work is to investigate the reasons for such differences and explain the corrosion behavior observed in a simulated marine environment by studying the micromorphological and microstructural characteristics of the flame-sprayed coatings.

2 Experimental procedure

The substrates used were commercial, hot-rolled low-carbon steel sheets AISI 1010 ($50 \times 70 \times 4$ mm^3 in size), which were sandblasted with 0.1–1.0 mm alumina particles before the coating procedure. The chemical composition of the substrates is summarized in Table 2 [13].

The coating deposition took place with a METCO wire flame-spray gun. Zinc was fed in the form of a Metco zinc wire (∅ 3.16 mm) with feed rate equal to 0.48 m/min. The fuel gas consisted of oxygen and acetylene with flow rates equal to 43 l/min and 19 l/min, respectively, in order to provide the necessary flame temperature for the wire melting. The spraying distance was 130 mm.

For the examination of the surface morphology of the coating, the samples were initially observed at low magnification with a Zeiss M8 stereoscope connected with a digital camera. Afterwards, for morphological observations and thickness measurements, cross sections were cut from each specimen, mounted in bakelite and polished with a 2000-grit paper and 5 μm alumina emulsion. Then, observations of the polished samples were made using an Olympus BX60 optical microscope connected with a digital CCD camera, JVC TK-C1381, while a 20 kV JEOL 840A SEM equipped with an OXFORD ISIS 300 EDS analyzer and the necessary software was used for detailed study, in order to perform point microanalysis or chemical mapping of the surface under examination.

Table 2 Chemical composition (wt%) of AISI 1010 specimens.

Fe	C	Mn	S (max)	P (max)
balance	0.08–0.13	0.30–0.60	0.05	0.0140

To determine the structural characteristics of the examined coatings, as well as the resulted phases, X-ray diffraction (XRD) was used with a 2-cycle SEIFERT 3003 TT diffractometer (Cu K_α radiation). Selected specimens were also observed with conventional transmission electron microscopy (CTEM) using a 100 kV JEOL 100CX TEM.

TEM microscopy was used because it can identify phases by electron diffraction even if they exist only in a small portion in the material and are "invisible" to the X-rays. Further, due to the small diameter of the electron beam of a TEM, the different phases among adjacent crystallites in a multiphase and polycrystalline material can be easily distinguished.

Corrosion tests were performed in a salt-spray chamber SC-450, where the samples were exposed at 40 °C in a fog of a 5 wt% solution of NaCl in deionized water. The exposure period was 8 days. The corroded samples, after the necessary pretreatment which was previously mentioned, were examined with SEM and EDS.

3 Results and discussion

3.1 Examination of the coating morphology

Optical microscopy and SEM were used for the preliminary examination of the coatings surface. Figure 1 presents typical micrographs, from which it is clear that the coating surface is extremely rough. This phenomenon is an inherent characteristic of thermal-sprayed coatings because not only liquid but also partially melted zinc droplets reach the

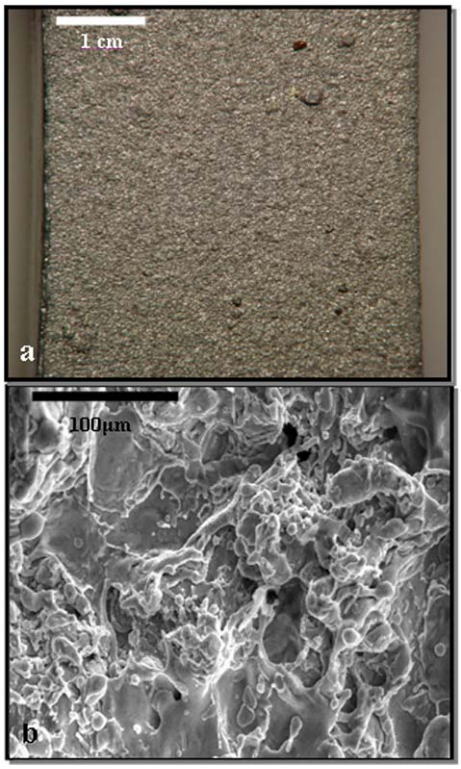

Figure 1 Stereoscopic photograph (a) and planview SEM micrograph (b) of the coating surface.

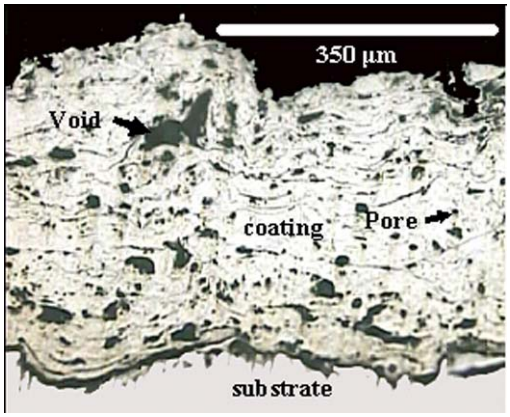

Figure 2 Cross-sectional optical micrograph of thermal-sprayed coating.

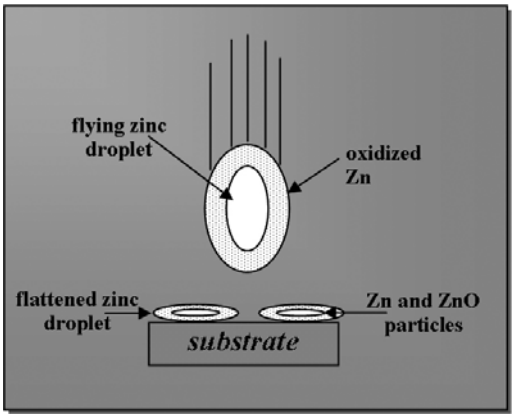

Figure 3 Schematic representation explaining the morphology and the formation of ZnO during the zinc droplet flight in the as deposited coating.

surface of the substrate during the coating process. Solidification is due to fast cooling of the droplets during their flight. The solid material is incorporated in the coating with very small changes of their shape. Consequently, it is impossible for the resultant surface to be even or uniform. In any case the surface relief depends on several experimental parameters such as the wire feedstock rate, the viscosity of the liquid metal and momentum of the particles at impact. As a result, high superficial roughness is unavoidable [2].

Nevertheless, more information could be gathered from the observation of cross-sectional micrographs. As Fig. 2 shows, the average thickness of the coating was about 350 μm. This value is much higher than the average thickness of hot-dip (~80 μm [1]) and electroplated coatings (~20 μm [8]). This phenomenon is attributed to the high zinc feed rate in the flame, as a lower rate results in the vaporization and burning of the metal because there is not enough mass to absorb the heat offered by the flame. Hence, the formation of thinner coatings is not possible.

Furthermore, Fig. 2 reveals the existence of lamellic formations of different sizes and shapes throughout the coating. These formations are the result of the successive stacking of the sprayed zinc droplets in molten, semimolten or even solid state when reaching the substrate. The solid particles undergo very low deformation during their impact on the already formed coating and consequently smaller lamellae are formed. By contrast, the liquid droplets flow extensively on impact and form elongated splats (Fig. 3). The combination of these particles finally results to the morphology observed in Fig. 2.

The previously described mechanism is also responsible for the existence of pores and voids in the mass of the coating. Partially or totally solidified zinc droplets that arrive on the surface of the substrate or on the previously formed coating may not fit exactly the existing surface morphology as their shape is constant. As a result they create pores. This phenomenon is known as gas porosity [14, 15]. Merging or communication of the as-formed pores results to voids, which are characterized by much larger dimensions. The formation of voids is enhanced by the shrinkage of liquid zinc upon solidification [16]. The examination of several micrographs of the as-cast coatings showed that pores and voids are randomly scattered in the coating mass. The average porosity was calculated at about 14%, which is relatively high. However, there are only very few pores that communicate creating diffusion paths for corrosive elements and are not likely to contribute negatively to the anticorrosive performance of the coating.

3.2 Examination of the coating composition and microstructure EDS analysis of several areas of the cross-sectional profile of the samples revealed that the coating is composed of pure zinc. The examination of the Fe/Zn interface showed that there are no Fe–Zn phases. Hence, zinc does not diffuse into the ferrous substrate, in contrast with other zinc coatings [1, 8]. This phenomenon is explained through the fact that cooling of melted particles on the substrate is very rapid and solidification is rather fast. The diffusion between two solid surfaces, as in this case, is a very slow process and is not likely to have happened under the herein experimental conditions. Hence, the bond between the substrate and the coating is only mechanical and neither metallurgical nor chemical, as in the case of other coatings [1, 8].

In order to determine the structure of the coatings XRD analysis was used. The XRD patterns of the coating was detected from the surface to the interior of the coating, with each layer being carefully removed by using 1200-grit paper. The as-received XRD patterns are presented in Fig. 4. In every case, the reflections of pure zinc were detected [17]. Peaks referring to Fe–Zn phases or other compounds were not recorded, as was expected following the EDS results.

However, the presence of metallic oxides trapped inside the coating is reported in several detailed studies of thermal-sprayed coatings of other metals [18]. These oxides are due to the oxidation of the spray particles in the combustion chamber of the spray gun because of the pres-

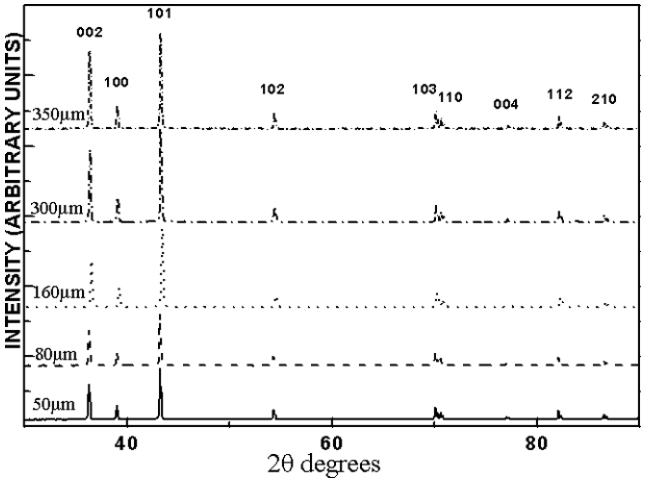

Figure 4 XRD patterns at different depths of the coating, where only Zn peaks are detected.

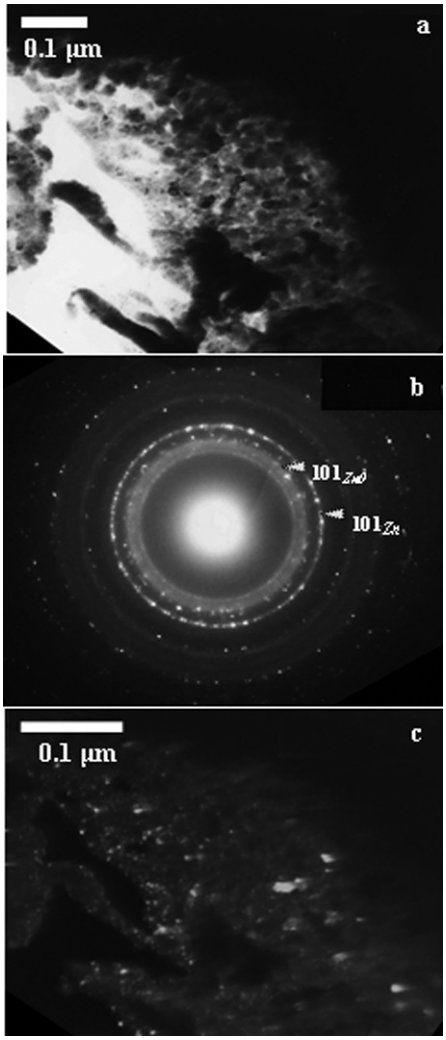

Figure 5 Bright-field TEM image (a) with the corresponding diffraction pattern (b) and a related dark-field image (c) taken from the dull circular zone.

ence of oxygen from the fuel mixture. In this study, zinc particles are also oxidized from the surrounding oxygen during their flight (Fig. 3), since zinc is a very reactive metal and its liquefaction enhances its chemical activity.

There are numerous parameters that affect this phenomenon, such as the oxygen/fuel ratio, the flame temperature, the particle velocity and the stand-off distance of the flame-spray gun [18]. In addition, the turbulent mixing of the liquid metal during the particle flight destroys the continuity of the oxide layer and distributes its pieces through out the whole mass of the flying droplet. Furthermore, the oxide film is smashed at the impact of the droplet on the substrate and is mixed in the core of the droplet. Conseuently, the presence of zinc oxides in the zinc coating seems to be highly probable. Nevertheless, neither EDS nor XRD revealed the presence of oxygen compounds.

This limitation of the above-mentioned techniques led to the examination of the coating with TEM. This investigation revealed the presence of Zn grains (PDF#65-5973 [17]) with a great variety of sizes (from 40 nm up to 2 μm) observed in the whole studied area. Figure 5a shows a typical bright-field TEM micrograph with the corresponding diffraction pattern (Fig. 5b) together with a related dark-field image (Fig. 5c). As it is seen in the diffraction, apart from the normal spots, other spots forming a shallow and almost diffuse circular zone appear. Figure 5b shows a characteristic case, where the electron diffraction pattern was taken using a large selected-area aperture. The individual and defined spots forming the classical polycrystalline rings belong to zinc crystallites, while the other ones forming the dull zone are attributed to ZnO nanoparticles. The broadness of the ZnO ring is caused by the off-stoichiometric ZnO_x phase (for example PDF#13-0311 [17]) and the absence of the defined spots inside the zone is attributed to its nanocrystallinity. In fact, the dark-field image (Fig. 5c) taken from the ZnO_x zone reveals that the size of the nanoparticles ranges from 2 nm to 20 nm. Finally, in some limited cases, as is shown in Fig. 6, some spots are attributed to the ZnO_2 phase. Obviously the small volume fraction of the oxides in the Zn coating is the reason that prohibited XRD and EDS from their detection.

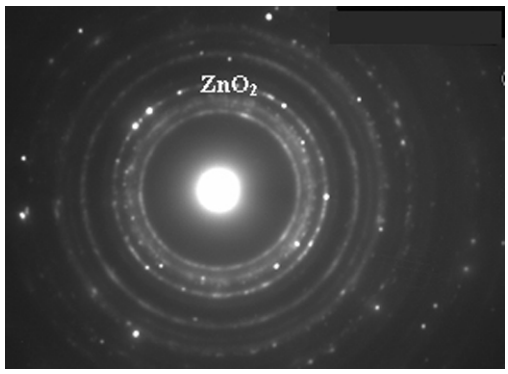

Figure 6 ED patterns consisting of polycrystalline rings showing the existence of Zn, ZnO and ZnO_2 grains.

The formation of zinc oxides is due to the previously described procedure. The small size of the as-formed grains could be explained by the very low flight time [19], while the growth of nanocrystaline Zn grains could be attributed to very fast solidification of the metal droplets, especially along their circumference [20]. The as-formed solid film impedes heat transfer and consequently the solidification of the interior of the droplets is slower, resulting in the growth of large grains.

3.3 Corrosion performance Several studies related to zinc corrosion are reported in the literature. In particular, they refer to electrochemical corrosion and high-temperature corrosion of zinc coatings and give significant quantitative corrosion results [9–11, 21, 22]. However, little work is related to zinc corrosion under accelerated simulated atmospheres in a salt-spray chamber, which is one of the herein examined subjects.

Figure 7a is a cross-sectional SEM micrograph of a zinc thermal-sprayed coating after 8 days in the salt-spray chamber. After this period the corrosive elements did not penetrate the whole thickness of the flame-sprayed coating and did not reach the protected ferrous substrate. By contrast, in the case of hot-dip coatings and zinc pack coatings the ferrous substrate is exposed after the same exposure period [23, 24]. The chemical mappings (Fig. 7) show that chlorine (Fig. 7d), which is the most aggressive corrosive element in a marine atmosphere, is restricted in the upper part of the coating, while the zinc concentration (Fig. 7e) is at a high level in the areas near the interface. Oxygen is inserted in the coating in small amounts during the deposition process, as was mentioned previously and at higher amounts during the corrosion procedure. This explains the oxygen chemical mapping image of Fig. 7c, where oxygen compounds are dispersed through the whole coating with higher concentration in the upper areas of the coating and much lower dipper in the mass of the coating. From these remarks it can be concluded that the substrate is not affected by corrosive elements after 8 days of corrosion and in any case it seems that the thermal-sprayed coatings exhibit a better corrosion performance than hot-dip galvanized and zinc pack coatings. Thermal-sprayed coatings are uniformly corroded with a diffusion mechanism. Neither pitting nor intergranular corrosion were observed, although these mechanisms are predominant in hot-dip galvanized and zinc pack coatings [23, 24]. Consequently the porosity and the trapped oxides do not affect the corrosion performance of the coating. As a general conclusion it can be safely claimed that zinc flame-sprayed coatings are a promising alternative industrial solution as they combine adequate anticorrosion performance, elevated production rate and low application cost. Thus, they can be applied in all cases where galvanized steels are used such as in marine environments and industrially polluted atmospheres.

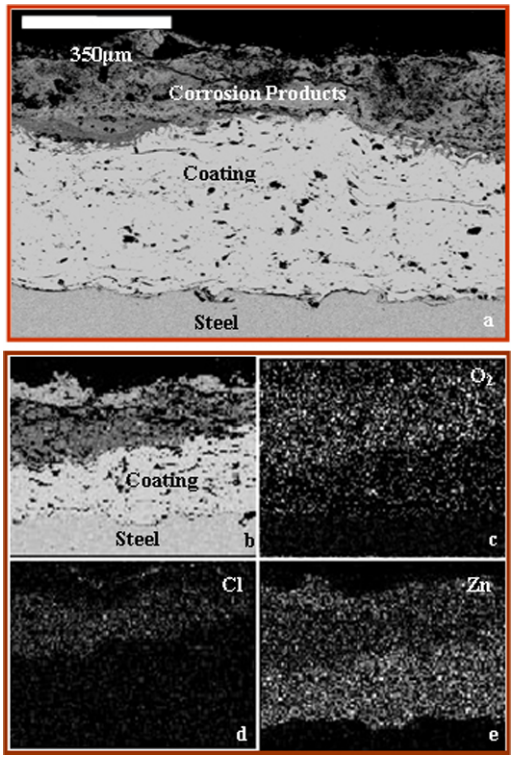

Figure 7 SEM micrograph (a) of the cross-sectional general view of a corroded sample after 8 days in the salt-spray chamber, along with chemical mapping of a particular area (b) showing the distribution of oxygen (c), chlorine (d) and zinc (e).

4 Conclusions In this work a morphological and structural study of flame sprayed zinc coatings was performed. It was found that zinc thermal-sprayed coatings are characterized by a very rough surface and large thickness. Morphologically they are composed of a lamellic structure with high porosity. All these observations are attributed to the deposition method. Consequently, from a morphological point of view, there are large differences between "traditional" zinc coatings and the thermal-sprayed coatings.

With regard to the composition, the coating was found to consist of pure zinc, along with a small amount of Zn oxides trapped in its mass. The formation of these oxides is due to the coating procedure as liquid particles tend to oxidize from the oxygen of the flame during their flight from the flame-spray gun to the coating. Furthermore, from the TEM observation it was found that the grains of Zn have different dimensions ranging from large crystals to nanocrystals, while Zn oxides form nanoparticles.

Finally, accelerated corrosion tests showed that after 8 days of exposure the corrosive elements had penetrated in the Zn coating but had not reached the ferrous substrate as in the case of hot-dip galvanized and pack coatings. Hence, it is deduced that thermal-sprayed coatings are more resistant.

References

[1] A. R. Marder, Prog. Mater. Sci. **45**, 191 (2000).
[2] R. C. Tucker, Thermal Spray Coatings, Vol. 5 (ASM International, USA, 1996).

[3] J. D. Olivas, C. Mireles, E. Acosta, and E. V. Barrera, Thin Solid Films **299**, 143 (1997).
[4] A. Forn, J. A. Picas, and M. J. Simon, J. Mater. Process. Technol. **52**, 143–144 (2003).
[5] I. Ozdemir, C. Tekmen, S. C. Okumus, and E. Celik, Surf. Coat. Tech. **174/175**, 1101–1105 (2003).
[6] S. Sampath, X. Jiang, G. X. Wang, and A. Vardelie, in: Proc. of the 9th Symp. on Surface Engineering, Vol. 20 (CIMTEC, Florence, Italy, 1998), p. 259.
[7] Engineering and Design-Thermal Spraying: New Construction and Maintenance, CECW-ET, Engineer Manual 1110-2-3401, Department of the Army, U.S. Army Corps of Engineers, Washington, 1999.
[8] Zinc coatings, American Galvanizing Association, Englewood, Colorado, 2000.
[9] X. G. Zhang, Corrosion and Electrochemistry of Zinc (Plenum Press, New York, 1996).
[10] G. Vourlias, N. Pistofidis, D. Chaliambalias, K. Chrissafis, El. Pavlidou, and G. Stergioudis, J. Therm. Anal. Calor. **87**, 401–409 (2007).
[11] G. Vourlias, N. Pistofidis, K. Chrissafis, and G. Stergioudis, J. Therm. Anal. Calor. **90**, 769–775 (2007).
[12] G. Vourlias, N. Pistofidis, El. Pavlidou, and K. Chrissafis, J. Therm. Anal. Calor. **90**, 777–782 (2007).
[13] ASM Metals Handbook, Vol. 9 (ASM International, USA, 1985), pp. 297–298.
[14] C. C. Berndt, W. Brindley, A. N. Goland, H. Herman, D. L. Houck, K. Jones, R. A. Miller, R. Nieser, W. Riggs, S. Sampath, M. Smith, and S. Spanne, J. Therm. Spray Technol. **1**(4), 341 (1992).
[15] J. R. Finke and W. D. Swank, Proc. Int. Thermal Spray Conf., Orlando, USA, 1992, p. 513.
[16] M. Flemings, Solidification Processing (McGraw Hill, New York, 1974).
[17] PC Powder Diffraction Files, JCPDS-ICDD, 2000.
[18] M. P. Planche, B. Normand, H. Liao, G. Rannou, and C. Coddet, Surf. Coat. Technol. **157**, 247–256 (2002).
[19] H. Sun and X. Pan, J. Mater. Res. **19**(10), 3062–3067 (2004).
[20] V. V. Sobolev, Mater. Lett. **36**, 123–127 (1998).
[21] X. Liu, J. Xiong, J. Cao, and Y. Zuo, J. Chem. Ind. Eng. **58**(9), 2288–2292 (2007).
[22] R. Ramanauskas, L. Gudavičiūtė, R. Juškėnas, and O. Ščit, Electrochim. Acta **53**(4), 1801–1810 (2007).
[23] G. Vourlias, N. Pistofidis, G. Stergioudis, E. Pavlidou, and D. Tsipas, phys. stat. sol. (a) **201**(7), 1518–1527 (2004).
[24] N. Pistofidis, G. Vourlias, D. Chaliampalias, E. Pavlidou, G. Stergioudis, and E. K. Polychroniadis, Surf. Interface Anal. **38**, 252–254 (2006).